Cell Insight 3 (2024) 100198

Contents lists available at ScienceDirect

Cell Insight

journal homepage: www.journals.elsevier.com/cell-insight

Research Article

The methyltransferase SETD3 regulates mRNA alternative splicing through interacting with hnRNPK

Yue-Yu Kong [a], Wen-Jie Shu [b], Shuang Wang [a], Zhao-Hong Yin [a], Hongguo Duan [a], Ke Li [a], Hai-Ning Du [a,*]

[a] Hubei Key Laboratory of Cell Homeostasis, College of Life Sciences, TaiKang Center for Life and Medical Sciences, Frontier Science Center for Immunology and Metabolism, RNA Institute, Wuhan University, Wuhan, 430072, China
[b] School of Basic Medical Sciences, Xi'an JiaoTong University, Xi'an, 710049, China

HIGHLIGHTS

- SETD3 interacts with a variety of splicing-associated proteins.
- SETD3 regulates pre-mRNA exon skipping mainly through association of hnRNPK.
- SETD3 and hnRNPK coregulate FNIP1 splicing to promote mitochondrial biogenesis.

GRAPHICAL ABSTRACT

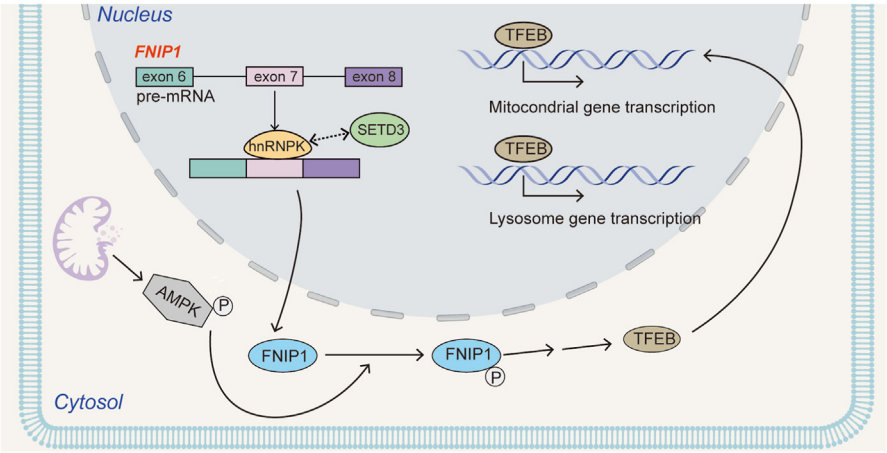

ARTICLE INFO

Keywords:
SETD3
RNA splicing
RBPs
hnRNPK
FNIP1

ABSTRACT

The methyltransferase SETD3 is an enzyme essential for catalyzing histidine-73 methylation on β-Actin, thereby promoting its polymerization and regulating muscle contraction. Although increasing evidence suggests that SETD3 is involved in multiple physiological or pathological events, its biological functions remain incompletely understood. In this study, we utilize *in situ* proximity labeling combined with mass spectrometry analysis to detect potential interacting partners of SETD3. Unexpectedly, we find that many splicing factors are associated with SETD3. Genome-wide RNA sequencing reveals that SETD3 regulates pre-mRNA splicing events, predominantly influencing exon skipping. Biochemical and bioinformatic analyses suggest that SETD3 interacts with hnRNPK, and they collaboratively regulate exon skipping in a common subset of genes. Functionally, we demonstrate that SETD3 and hnRNPK are required for retention of exon 7 skipping in the *FNIP1* gene. This promotes FNIP1-mediated nuclear translocation of the transcription factor TFEB and the subsequent induction of lysosomal and mitochondrial biogenesis. Overall, this study uncovers a novel function of SETD3 in modulating mRNA exon splicing.

* Corresponding author.
E-mail address: hainingdu@whu.edu.cn (H.-N. Du).

https://doi.org/10.1016/j.cellin.2024.100198
Received 26 June 2024; Received in revised form 18 August 2024; Accepted 18 August 2024

1. Introduction

As a subfamily of methyltransferases, SET domain-containing proteins are involved in various chromatin-based biological processes, including transcription, replication, and chromosome maintenance to development, differentiation, and aging (Black et al., 2012; Cornett et al., 2019; Herz et al., 2013; Husmann & Gozani, 2019; Zhang et al., 2015).

Recently, a new subclass of methyltransferases responsible for transferring a methyl moiety on the nitrogen of the imidazole rings of histidine residue, including SETD3, METTL9, METTL18, and CARNMT1, have been discovered (Cao et al., 2018; Davydova et al., 2021; Jakobsson, 2021; Shimazu et al., 2023; Wilkinson et al., 2019; Zhao et al., 2023). Considerable attention has been gained to this type of methylation through the characterization of the first metazoan histidine methyltransferase, SETD3. SETD3 is required for regulating β-actin polymerization and smooth muscle contraction by methylating histidine 73 on β-actin across vertebrates (Kwiatkowski et al., 2018; Wilkinson et al., 2019). Consequently, depletion of *Setd3* causes primary dystocia in female mice (Wilkinson et al., 2019). Very recently, our group revealed a role of SETD3 in DNA replication by methylating histidine 459 on MCM7, a subunit of the minichromosome maintenance (MCM) 2–7 complex (Duan et al., 2024). Besides its enzymatic activity-dependent functions, the identification of numerous SETD3 interactors indicates that SETD3 is also involved in various biological and pathological processes, including viral pathogenesis (Diep et al., 2019), carcinogenesis (Shu & Du, 2021), cellular apoptosis (Abaev-Schneiderman et al., 2019), post-stroke depression (Feng et al., 2022), and mouse endoderm differentiation (Alganatay et al., 2024), which may be independent of its histidine methylation activity. These versatile functions highlight the significance of further studying SETD3.

Alternative RNA splicing, an enzymatic process of excising introns from messenger RNA precursors (pre-mRNA) to generate multiple mature transcripts from a single gene, plays a pivotal role in enhancing proteome diversity and fine-tuning gene expression (Wright et al., 2022). Dysregulated RNA splicing contributes to nearly all types of cancers (Escobar-Hoyos et al., 2019). Although the spliceosome, a large RNA-protein complex, predominantly catalyzes splicing, various splicing factors are also essential for the dynamic recruitment of spliceosome proteins to consensus splice sites (Rogalska et al., 2023). Two common families of splicing factors, serine/arginine-rich splicing factors (SR proteins) and heterogeneous nuclear ribonucleoproteins (hnRNPs), regulate splicing events in a context-dependent manner. For instance, SR proteins bind to exonic splicing sequences to enhance splicing, whereas hnRNPs bind to exonic splicing sequences to inhibit splicing (Busch & Hertel, 2012). Notably, several methyltransferases, including m^6A RNA methyltransferase METTL16 (Mendel et al., 2021), lysine methyltransferase SETD5 (Sessa et al., 2019), and arginine methyltransferase PRMT5 and PRMT7 (Li et al., 2021; Sachamitr et al., 2021), have been reported to function in RNA splicing. However, little is known whether histidine methyltransferases are involved in this process.

In this study, we uncover that SETD3 interacts with pre-mRNA splicing factors. Knockdown of *SETD3* leads to alteration of mRNA splicing events, particularly enhancing exon skipping. Biochemically, we find that SETD3 physically associates with hnRNPK to collaboratively regulate post-transcriptional processing of pre-mRNA in an activity-independent manner. We find that SETD3 and hnRNPK coregulate FNIP1 exon 7 skipping; retention of this exon is required for FNIP1-mediated nuclear translocation of the transcription factor TFEB and subsequent induction of lysosomal and mitochondrial biogenesis. Our results highlight a novel role of SETD3 in preserving the fidelity of mRNA exon splicing.

2. Results

2.1. SETD3 associates with numerous splicing-related proteins

To explore new roles of SETD3, we sought to identify its potential interacting proteins. For this purpose, we employed proximity labeling by biotin addition in HeLa S3 cells expressing SETD3-TurboID or an empty TurboID vector. Cell lysates were subjected to immunoprecipitation, and two independent mass spectrometry (MS) experiments were conducted (Fig. 1A). A total of 1746 proteins were identified in the samples expressing SETD3-TurboID, which were not present in the samples expressing the TurboID vector (Fig. 1B). Kyoto Encyclopedia of Genes and Genomes (KEGG) analysis revealed that multiple splicing factors were among the top candidate in the SETD3 interactome (Fig. 1C). Supporting this, 77 splicing-related factors were present in both MS experiments (Fig. 1D). Interestingly, spliceosome components, such as U2/U4/U5/U6 snRNPs, the Prp19 complex, and RNA helicases were detected. Additionally, numerous hnRNP proteins, which function as splicing co-suppressors, were also enriched (Fig. 1E). Consistently, splicing-related proteins or RNA binding proteins (RBPs) were enriched according to different Gene Ontology (GO) analyses, including biological process (BP), molecular function (MF), and cellular component (CC) pathway enrichment, indicating that splicing-related proteins might be the main interacting partners of SETD3 (Figs. S1A–C). Ranking the detected peptide numbers of the SETD3 interactors, the top 10 candidates included five different hnRNP proteins (Fig. 1F). The results indicate a potential functional connection of SETD3 with splicing proteins.

2.2. SETD3 regulates pre-mRNA splicing

Given that many splicing factors are among the interacting partners of SETD3, we speculate that SETD3 might function in the post-transcriptional processing of pre-mRNA. To test this, SETD3 was depleted in HeLa S3 cells using small interfering RNA (siRNA) oligos, and the knockdown efficiency was examined in three biological samples (Fig. 2A). To assess the impact of SETD3 on pre-mRNA splicing, genome-wide RNA-sequencing (RNA-seq) was employed to analyze SETD3-mediated splicing variation events. Heatmap exhibited strong repeatability in each group (Fig. S2A). As expected, knockdown of *SETD3* led to global splicing changes, with a total of 3463 alternative splicing (AS) events detected, 69% of which (2,396) affected exon skipping (Fig. 2B). Among these exon-skipping (ES) events, knockdown of *SETD3* resulted in nearly two-thirds of exons (1,501) being skipped (Fig. 2C). Consistently, inspection of individual genes revealed apparent skipped exons of several genes in SETD3-depleted cells (Fig. 2D and E). More importantly, the differential alternative AS events were not predominantly due to changes in gene expression, as only 817 differential expressed genes (DEGs, $|\mathrm{Log_2(Foldchange)}| > 1$, P value < 0.05) were present upon *SETD3* depletion (Fig. S2B). Of note, only 33 genes overlapped between the DEGs and alternative splicing genes (ASGs), implying that gene expression changes are not the primary driver of the alternative splicing regulated by SETD3 (Fig. S2C). Supporting this, GO analysis of 814 DEGs suggested that SETD3 does not affect expression of splicing-related genes (Fig. S2D and Table S1). Furthermore, Surveying the 77 SETD3-associated splicing genes showed no significant changes in gene expression upon *SETD3* knockdown, indicating that the splicing events influenced by SETD3 are not attributed to altered expression of splicing factors (Fig. S2E).

To further validate the occurrence of RNA exon skipping *in vivo*, we quantified the unspliced and spliced isoforms using designed exon-exon primers for four candidate genes. Reverse transcript-PCR (RT-PCR) analysis showed that knockdown of *SETD3* induced an obvious decrease in alternative exon-included signal and an increase in the exon-excluded signal without affecting the levels of *GAPDH* (Figs. S2F–G). Collectively, these results indicate that SETD3 directly regulates mRNA splicing, particularly crucial for exon inclusion.

2.3. Direct interaction between SETD3 and nucleic acids is not observed

Given the impact of SETD3 on regulating mRNA splicing, we speculate that SETD3 might act as an uncharacterized splicing factor. However,

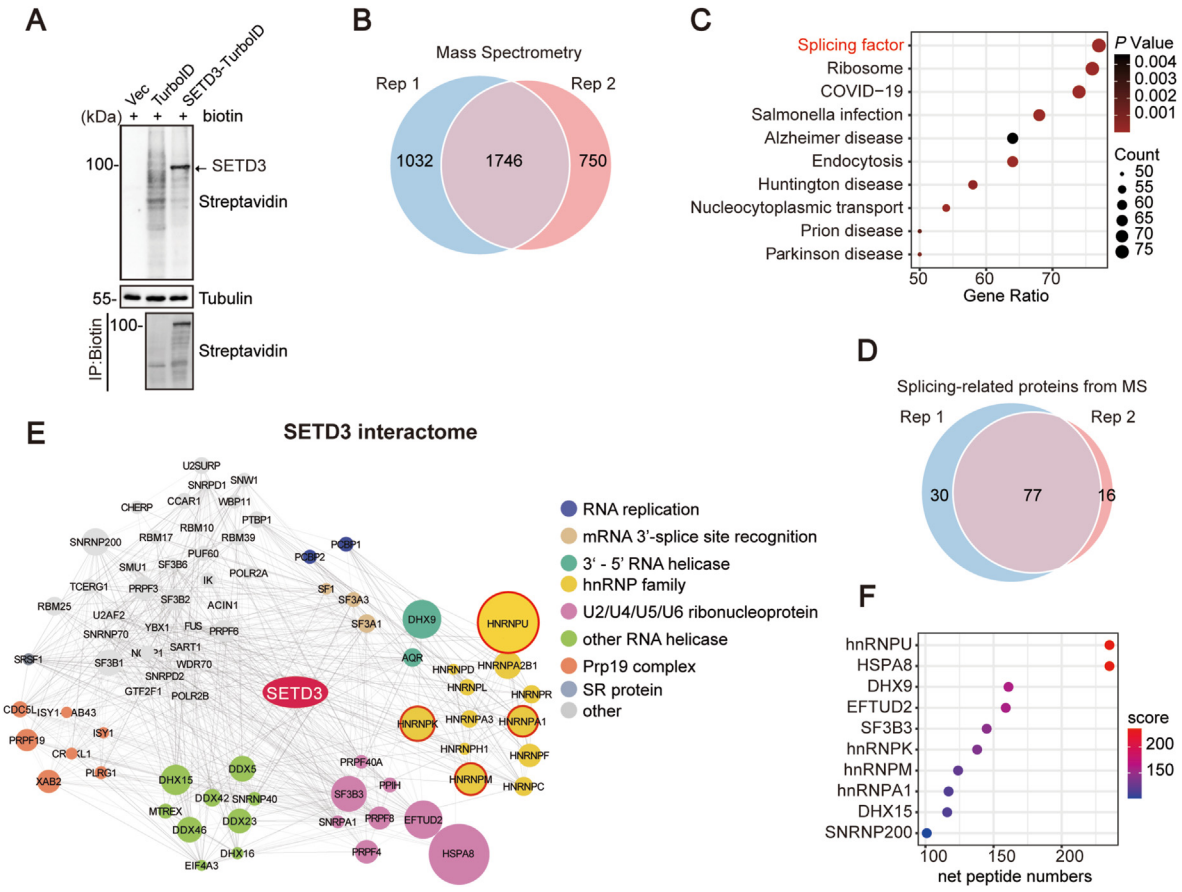

Fig. 1. SETD3 interacts with splicing-associated proteins. (**A**) Western blotting detected the interacting proteins of SETD3 by immunoprecipitation of biotin-coupled SETD3 in HeLa S3 cells expressing the TurboID vector or *SETD3*-TurboID. (**B**) Venn diagram showed potential SETD3-interacting proteins identified in the two independent MS experiments. (**C**) KEGG analysis showed the top 10 categories of SETD3 interactome. (**D**) Venn diagram displayed the splicing-related proteins identified in the two independent MS experiments. (**E**) Overview of 77 potential SETD3-interacting proteins belonging to different splicing factor groups, and different colors represent different groups of mRNA splicing functions. (**F**) Bubble diagram represented the number of peptides among the top 10 SETD3-interacting splicing proteins identified by MS.

structural prediction of the RNA recognition motif in SETD3 showed no obvious signatures. Therefore, we decided to experimentally explore the interaction between SETD3 and RNA. We employed a simplified and efficient method called GoldCLIP (gel-omitted ligation-dependent UV-crosslinking and immunoprecipitation) as described previously (Gu et al., 2018). In this system, a HaloTag was fused to the N-terminus of SETD3, with a 3 × TEV cleavage site and a 2 × StrepII were engineered in between. A PTB-fusion protein served as a positive RNA-binding control. HeLa S3 cells stably expressing the fusion proteins or an empty vector were crosslinked by ultraviolet light, and SETD3 or PTB protein was immunoprecipitated using HaloTag beads. After protein digestion and de-crosslinking, protein-bound RNAs were released and quantified using a spectrometer (Fig. 3A). Despite that we observed abundant RNA signals with PTB, both SETD3 and the negative control displayed rare RNA signals, suggesting that SETD3 may not bind RNA directly (Fig. 3B).

It has been demonstrated that SET-domain containing protein SETD2 co-transcriptionally regulates RNA splicing by methylating histone H3 Lys36 (Bhattacharya et al., 2021). We inferred that SETD3 might couple transcription and RNA splicing by engaging in chromatin regulation. Thus, we next examined whether SETD3 could associate with chromatin. To enhance the enrichment intensity of endogenous SETD3, chromatin immunoprecipitation followed by sequencing (ChIP-seq) was performed in HeLa S3 cells bearing wild-type *SETD3* alleles tagged with a 3 × Flag-HA tag (SETD3-FH), where the HA tag could be used to monitor the occupancy of SETD3 in genome loci. After normalized SETD3-enriched peaks with control signals from HeLa S3 cell samples without insertion of the HA tag, we unexpectedly observed that SETD3 was particularly concentrated at centromere regions of every chromosome (Fig. 3C). To ascertain the accuracy of SETD3 localization, we re-analyzed the ChIP-seq dataset (GSE69839) of a known centromere protein, CENP-B (Earnshaw & Rothfield, 1985). Notably, the identified SETD3 peaks predominantly overlapped with the CENP-B peaks. To further confirm the direct association of SETD3 with centromeric DNA, an electrophoretic mobility shift assay (EMSA) was performed to examine the direct interaction of SETD3 with centromeric DNA. Purified recombinant SETD3 proteins carrying different epitope tags were incubated with a biotin-labelled centromeric double-strand DNA fragment (171 bp). As a positive control, the N-terminus (1–129 amino acids) of the CENP-B protein was also included (Muro et al., 1992). We noticed that CENP-B efficiently bound centromeric DNA in a dose-dependent manner. In contrast, the addition of SETD3 did not change the migration of the same DNA fragment (Fig. 3D and E). The data does not support a direct interaction between SETD3 and nucleic acids. However, it is notable that mass spectrometry of SETD3-TurboID identified three centromeric proteins— CENP-B, CENP-F, and CENP-V (Table S2). This suggests that centromeric enrichment of SETD3 is probably mediated via centromere-associated proteins. However, this occupancy appears unrelated to SETD3' role in mRNA splicing. In summary, we speculate that the interaction of SETD3 with splicing-related proteins is likely more important for mRNA splicing.

2.4. SETD3 regulates mRNA splicing by the association of hnRNPK

To explore whether SETD3 participates in post-transcriptional pre-mRNA processing through engagement with spliceosome proteins, we first analyzed the characteristics of skipping exon motifs regulated by SETD3. By defining the splicing events with $|\Delta IncLevel| > 0.1$ and FDR <0.05, cytosine-rich motifs were identified (Fig. 4A). Intriguingly, when we individually characterize the skipped exon motifs regulated by the top 10 candidate splicing proteins interacting with SETD3 (as shown in Fig. 1F), only hnRNPK, but not the others, exhibited similar cytosine-rich motifs as those regulated by SETD3 (Fig. 4B and S3). It should be noted that a large number of hnRNP proteins was identified as interacting with SETD3 by mass spectrometry (Fig. 1E). Although we revealed that hnRNPK and SETD3 share a highly similar exon motif, other proteins are also likely involved in SETD3-mediated mRNA splicing regulation. Based on these data, we conclude that hnRNPK may be the primary splicing factor collaborating with SETD3 in exon skipping events.

To validate the interaction between SETD3 and hnRNPK, we conducted *in vitro* co-immunoprecipitation and *in situ* proximity ligation assay (PLA) in living cells. First, we detected GFP-hnRNPK or Flag-SETD3 (knock-in tag) can co-immunoprecipitate with endogenous SETD3 or GFP-hnRNPK (Fig. 4C). Second, PLA showed colocalization of endogenous SETD3 and hnRNPK, confirming their association *in vivo* (Fig. 4D). Additionally, protein molecular docking was used to predict the physical interaction between SETD3 and hnRNPK. Interestingly, we found a potential interaction between a segment of hnRNPK containing its KI (K interaction) domain and a segment of SETD3 within its LSMT (large subunit methyltransferase)-like domain, both of which are known to interact with various proteins (Wilkinson et al., 2019; Yoo et al., 2006). Moreover, this strong interaction was supported by low free Gibbs free energy change (ΔG) and high binding affinity calculations (Fig. S4A). Altogether, these data suggest that SETD3 may physically interacts with hnRNPK.

To investigate whether hnRNPK could modulate the exon splicing events regulated by SETD3, HeLa S3 cells were transfected with siRNAs targeting *hnRNPK*, and Western blotting showed effective reduction of endogenous hnRNPK (Fig. 4E). In this scenario, we observed that reduction of hnRNPK promoted exon skipping of the same exons in SETD3-regulated genes, as examined by RT-PCR analysis (Fig. 4F). More importantly, RNA-seq analysis revealed that following *hnRNPK* knockdown, 1221 exons were skipped, with 304 of these also regulated by SETD3. This represents 24.9% of hnRNPK-regulated and 20.3% of SETD3-regulated exon skipped events (Fig. 4G). Furthermore, genome tracks of four candidates showed that they are co-regulated by both hnRNPK and SETD3 (Fig. 4H). Notably, double knockdown of *SETD3* and *hnRNPK* synergistically enhanced exon skipping of the *SPTAN1*, *AREL1*, and *FNIP1* genes compared to knockdown of *SETD3* or *hnRNPK* alone (Fig. 4I and J). The more pronounced exon skipping observed in the double knockdown cells implies that SETD3 may also influence RNA splicing through interacting with various splicing proteins. Nonetheless, these results indicate that SETD3 regulates exon skipping primarily by its interaction with hnRNPK.

To further examine whether SETD3 could directly methylate hnRNPK to mediate its activity, we conducted *in vitro* methyltransferase reactions using recombinant GST-SETD3 incubated with GST-hnRNPK or His-β-Actin. Liquid scintillation counting showed that only β-Actin, but not hnRNPK, exhibits robust ^{3}H-labelled SAM incorporation signals, even though an equal amounts of SETD3 were present in each reaction (Fig. S4B). Taken together, these data indicate that SETD3 associates with hnRNPK and cooperatively facilitates hnRNPK-mediated mRNA splicing in an enzyme-independent manner.

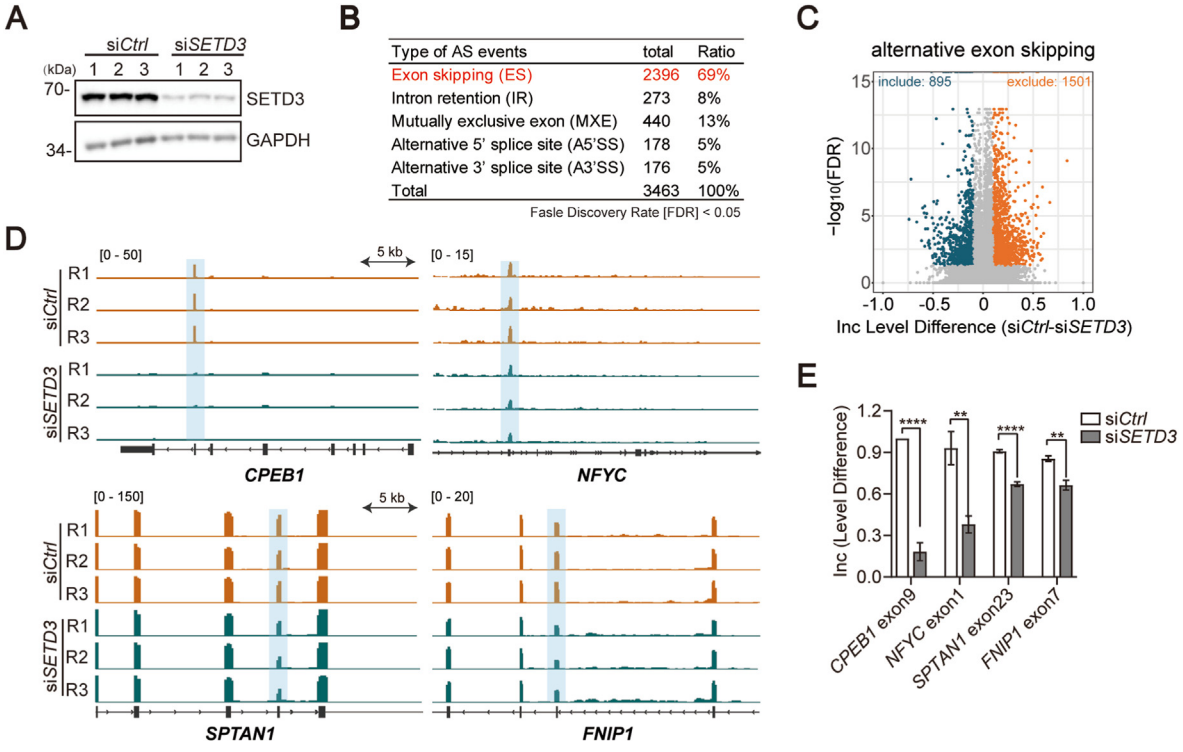

Fig. 2. SETD3 regulates pre-mRNA splicing. (**A**) Western blotting examined the levels of SETD3 after transfecting si*SETD3* oligos. (**B**) Statistical data summarized five categories of RNA alternative splicing events upon *SETD3* knockdown. "total" represents splicing events; and "Ratio" represents the proportions of each splicing event. (**C**) RNA-seq analysis of the effects of si*SETD3* in alternative mRNA splicing compared to the si*Control* (si*Ctrl*) samples. Volcano diagram showed alternative exon splicing events upon *SETD3* knockdown. (**D**) Genome browser tracks showed four representative splicing events occurred in si*SETD3* cells compared with si*Ctrl* cells. Three biological replicates of each sample are presented. (**E**) Data of representative splicing events shown in panel D were quantified. Error bars represent the mean ± standard deviation (SD) from three biological replicates with *P* values determined by two-tailed unpaired *t*-test. $^{**}P < 0.01$, $^{****}P < 0.0001$.

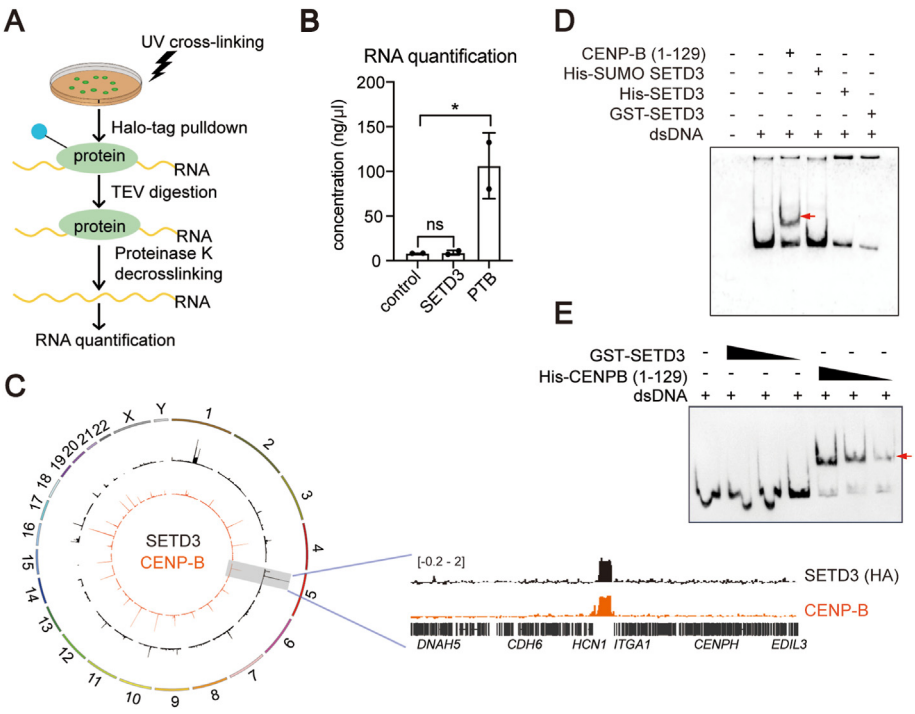

Fig. 3. Direct interaction between SETD3 and nucleic acids is not observed. (**A**) An experimental diagram showed the procedure for detecting protein-bound RNAs. (**B**) The concentrations of RNAs that bind to SETD3 or PTB protein were determined by a spectrometer. Two biological repeats were performed, and data are presented as mean ± SD with unpaired *t*-test. ns, not significant, $^{*}P < 0.05$. (**C**) Circular browser tracks depicted the genomic distribution of SETD3 (black) and CENP-B (orange) enrichment (left panel), while the linear tracks show the occupancies of these two proteins on Chromosome 5 (right panel). (**D-E**) EMSA examined the binding capacities of various SETD3 proteins or CENP-B (1–129 amino acid) fragment with synthetic DNA.

2.5. SETD3 is involved in lysosome and mitochondrial biogenesis by regulating FNIP1 exon skipping

We next attempted to explore the biological significance of alternative RNA splicing events co-regulated by SETD3 and hnRNPK. Using GO analysis, we observed that SETD3-regulated splicing genes are associated with small GTPase-mediated signal transduction (Fig. S5A). Interestingly, knockdown of *hnRNPK* leads to exon skipping in GTPase-related genes (Escobar-Hoyos et al., 2020). Indeed, GO analysis indicated that hnRNPK regulates GTP binding and GTPase activity-related pathways (Fig. S5B).

Previous study has illustrated that mitochondrial damage activates the adenosine monophosphate (AMP)-activated protein kinase (AMPK) to promote the biogenesis of lysosomal and mitochondrial genes (Malik et al., 2023). During this signaling transduction, the inactivation of GTP-activating protein (GAP) formed by AMPK-mediated phosphorylation of FNIP1 (folliculin-interacting proteins1) allows the nuclear translocation of TFEB (the transcription factor EB) from the cytosol, inducing transcription of lysosomal or mitochondrial genes (Fig. 5A, top panel). Notably, three out of five key phosphorylation sites of FNIP1, including Ser220, Ser230, and Ser232 (Malik et al., 2023), are located at the exon 7 coding region (Fig. 5A, bottom panel). It was shown that this exon can be skipped upon knockdown of *SETD3* or *hnRNPK* (Fig. 4H). Therefore, we hypothesize that SETD3 and hnRNPK might regulate the transcription of lysosomal or mitochondrial genes through *FNIP1* splicing. To test this hypothesis, HeLa S3 cells were treated with the mitochondria protonophore FCCP to induce mitochondria damage. Consistently, knockdown of *SETD3* or *hnRNPK* promoted *FNIP1* exon 7 skipping, regardless of FCCP treatment (Fig. 5B and C). However, knockdown of *SETD3* or *hnRNPK* compromised FCCP-induced TFEB translocation to the nucleus (Fig. 5D). Consequently, the expression of several lysosomal or mitochondrial genes, such as *COX6A1*, *IDH2* and *LAMP1*, is remarkably inhibited even in the presence of FCCP (Fig. 5E). Collectively, we propose that SETD3, together with hnRNPK, promotes lysosome and mitochondrial biogenesis by preventing *FNIP1* exon 7 skipping.

3. Discussion

SETD3 is a member of the SET domain-containing family, increasingly recognized for its key roles in various processes, including β-Actin polymerization and smooth muscle contraction, DNA replication, virus pathogenesis, tumorigenesis, post-stroke depression, and endoderm differentiation (Alganatay et al., 2024; Diep et al., 2019; Duan et al., 2024; Feng et al., 2022; Shu & Du, 2021; Wilkinson et al., 2019). Herein, we report its new function in mRNA splicing. Although SETD3 itself is unable to bind RNA and thus cannot directly exert alternative splicing, we find that SETD3 associates with splicing factors to primarily mediate exon skipping in many genes. Supporting our findings, previous studies have identified that SETD3 interacts with RNA splicing proteins (Abaev-Schneiderman et al., 2019; Admoni-Elisha et al., 2022). Specifically, we validate that one of hnRNP family proteins, hnRNPK, physically interacts with SETD3 *in vitro* and *in vivo*. More importantly, we illustrate that SETD3 and hnRNPK co-suppress exon 7 skipping of *FNIP1* gene to promote lysosomal and mitochondrial biogenesis. Overall, we conclude that SETD3 as a cofactor of splicing factors to preserve the fidelity of mRNA exon splicing.

In our study, MS-based proteomic analysis uncovers many SETD3-associated splicing factors, including the core spliceosome components for both early and late stages of splicing, U2/U4/U5/U6 ribonucleoproteins, and the Prp19 complex. Among these, the largest groups identified as SETD3 partners are hnRNPs (12 out of 77 proteins). HnRNPs represent a large group of RNA-binding proteins that contribute to various aspects of nucleic acid metabolism, including gene expression, mRNA stability, and alternative splicing (Geuens et al., 2016). Given the functional complexity of hnRNPs in regulating exon splicing, exon motif analysis was utilized to confine the co-regulators of SETD3. We found that SETD3 and hnRNPK share similar exon skipping motifs with cytosine-rich sequences, and knockdown of *hnRNPK* promotes exon skipping in a subset of common genes, which are also regulated by SETD3. Of note, previous studies have demonstrated that hnRNPK possesses three KH (K homology) domains, each of which binds to an RNA cytosine-rich box, and the

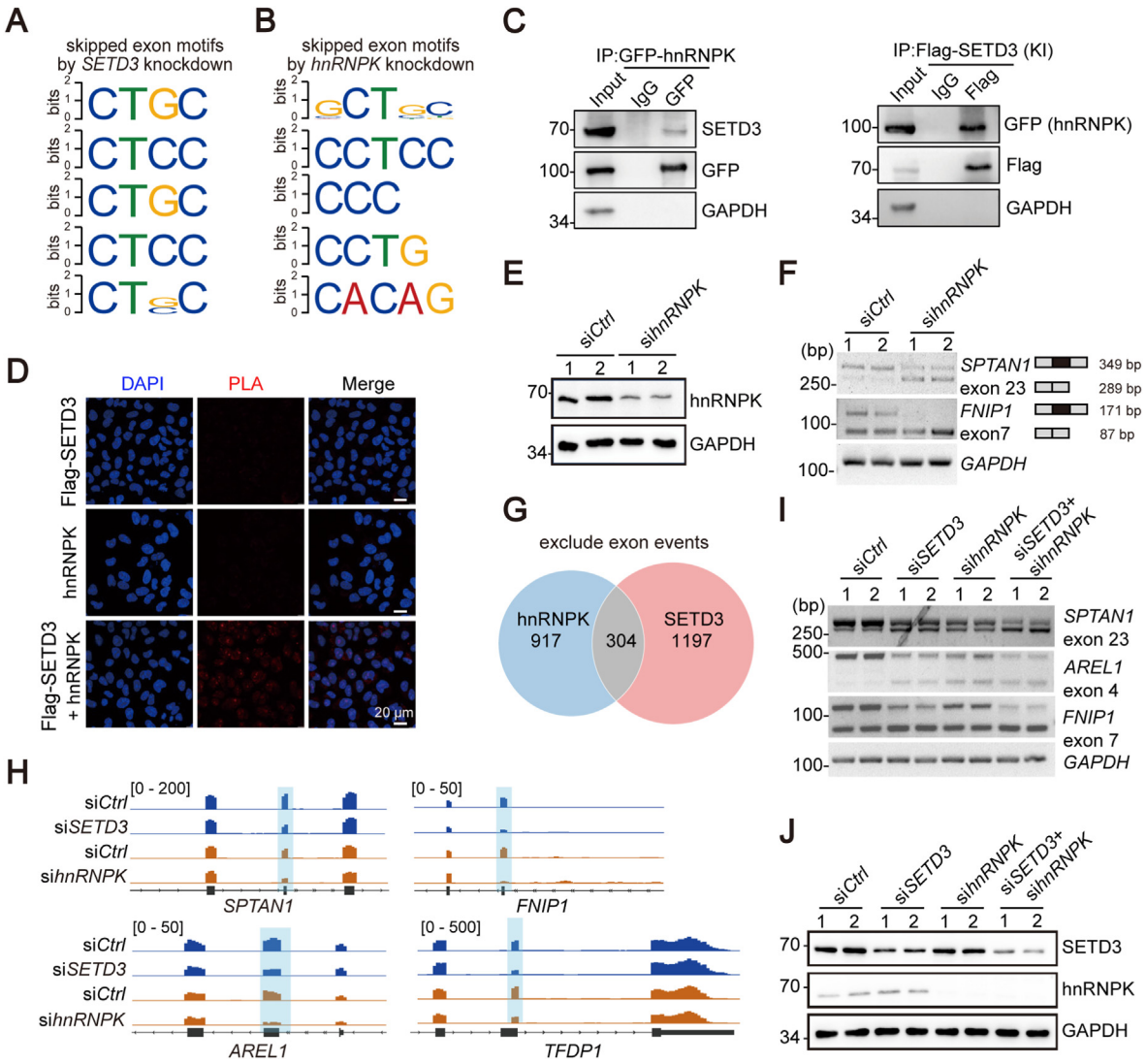

Fig. 4. The binding of SETD3 with hnRNPK cooperatively affects pre-mRNA splicing. (**A-B**) Illustration of skipped exon motifs upon *SETD3* (A) or *hnRNPK* (B) knockdown analyzed from GSA: HRA007736 or GEO: GSE114502. (**C**) Western blotting showed the interaction of endogenous SETD3 with exogeneous GFP-tagged hnRNPK in SETD3 knock-in cells. IgG serves as negative control. (**D**) PLA displayed the interaction of SETD3 and hnRNPK *in vivo*. (**E-F**) Western blotting examined the knockdown efficiency of *hnRNPK* upon siRNA transfection (panel E), and RT-PCR assays confirmed that hnRNPK regulates the same exon skipping events as SETD3 (panel F), and. (**G**) Venn diagram displayed the co-regulated exons upon knockdown of *hnRNPK* or *SETD3*. (**H**) Genome browser tracks showed four representative exon splicing events affected by both hnRNPK and SETD3. One from three biological replicates of each sample are presented. (**I-J**) RT-PCR assays examined that SETD3 and hnRNPK co-regulate exon skipping events of the indicated genes (panel I), and Western blotting examined the knockdown efficiency of *SETD3*, *hnRNPK*, or both upon siRNA transfection (panel J).

exon 7 of *FINP1* is a *bona fide* binding site of hnRNPK (Cai et al., 2020; Paziewska et al., 2004). Consistently, knockdown of *hnRNPK* alters post-transcriptional splicing, integrating in many signal transduction pathways by directly binding to certain mRNAs characterized with cytosine-rich exons (Escobar-Hoyos et al., 2020; Geuens et al., 2016; Ostrowski et al., 2004). Our work reveals that hnRNPK, in coordination with SETD3, regulates exon splicing of the *FINP1* gene, which prominently features cytosine-rich exons. Thus, these data further strengthen their functional connection in mRNA splicing. Since our results suggest that SETD3 and hnRNPK co-regulate mRNA splicing only in a subgroup of genes, we believe that SETD3 likely orchestrates with other interacting hnRNPs to mediate additional splicing events. More investigation needs to be done further.

It is intriguingly how SETD3 regulates alternative mRNA splicing, particularly exon skipping. Human SETD3 contains two conserved domains: a SET domain at the N-terminus and a LSMT (large subunit methyltransferase)-like domain at the C-terminus (Fig. S4A). This domain may interact with substrates and assist in their recognition and catalysis (Guo et al., 2019; Zheng et al., 2020). However, based on our experimental data and the structure of SETD3, we could not identify any direct interaction between SETD3 and nucleic acids (Fig. 3). Thus, it is unlikely that SETD3 regulates mRNA splicing through transcriptional or post-transcriptional processing of pre-mRNA. Furthermore, we excluded the possibility that SETD3 mediates mRNA splicing by affecting hnRNPK stability, as si*SETD3* does not alter hnRNPK protein level (Fig. 4J). Given that hnRNPK contains three conserved KH domains for RNA/DNA binding and the KI region between KH2 and KH3 involved in interaction with a variety of proteins, including SETD3, we speculate that SETD3 may assist hnRNPK in forming a complex with other hnRNPs to enhance its splicing efficiency (Shnyreva et al., 2000). The precise mechanism of SETD3 in mRNA splicing needs further investigation.

Abnormal expression levels of SETD3 are associated with liver tumorigenesis (Cheng et al., 2017; Xu et al., 2019; Zou et al., 2022), renal cell tumors (Pires-Luis et al., 2015), and breast cancer (Hassan et al.,

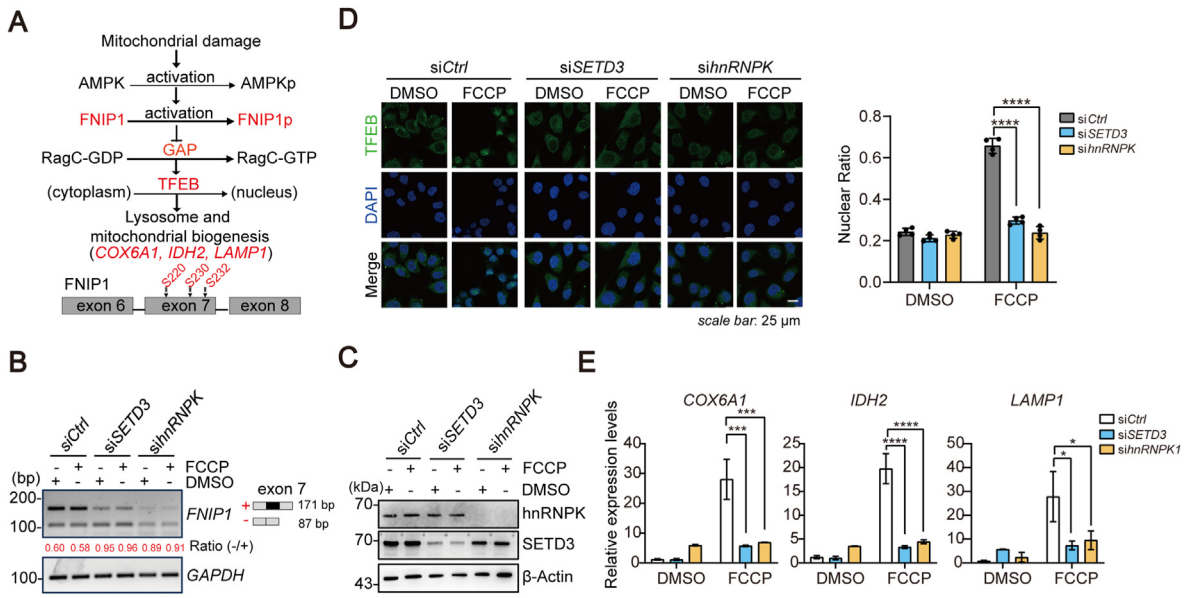

Fig. 5. SETD3 promotes lysosome and mitochondrial biogenesis by regulating exon skipping of *FNIP1* gene. (**A**) A schematic depicted, after mitochondrial damage, a signaling pathway transduced from AMPK-activated FNIP1 phosphorylation to nuclear translocation of TFEB, and subsequently facilitating lysosome and mitochondrial biogenesis (top panel). Three phosphorylation sites of FINP1 located at exon 7 were displayed (bottom panel), which are critical for nuclear translocation of TFEB. (**B-C**) Western blotting showed FCCP treatment does not further facilitate FNIP1 exon 7 skipping upon knockdown of SETD3 or hnRNPK (panel B), and the equal depletion efficiency of *SETD3* or *hnRNPK* in the presence DMSO or FCCP was examined (panel C). (**D**) Immunofluorescent images of representative cells transfected with the indicated siRNAs upon DMSO or FCCP treatment were displayed. TFEB localization (green) was shown. DAPI-stained for DNA (blue, left panel). *Scale bar*:25 μm. The ratios of nuclear translocation in the indicated samples were quantified (right panel). Each dot represents one area with >25 cells. (**E**) Expression levels of 3 representative genes were examined in cells transfected with the indicated siRNAs when treated with DMSO or FCCP. Data are presented from at least three independent replicates as mean ± SD with unpaired *t*-test. $^{*}P < 0.05$, $^{***}P < 0.001$, $^{****}P < 0.0001$.

2020). In addition, the expression levels of hnRNPs are altered in many types of cancer, often relevant for disease progression (Han et al., 2013; Rogalska et al., 2023). Our work links SETD3 with splicing factors and splicing events, suggesting a pathological role of SETD3-mediated mRNA splicing in cancers. Understanding the specific splicing events regulated by SETD3 would aid in investigating the molecular mechanisms underlying various cancers.

4. Materials and methods

4.1. Cell culture, transfections, and RNAi

Human HEK 293T (CRL-11268, ATCC, USA) and HeLa S3 (CCL-2.2, ATCC, USA) cell lines were cultured in Dulbecco's modified Eagle's medium (DMEM, FY30243A, Biofly, Wuhan) supplemented with 10% fetal bovine serum (A0500-3011, Cegrogen biotech, Germany), and 1% penicillin/streptomycin (PB180120, Procell, Wuhan). All cells were cultured at 37 °C with saturated humidity and an atmosphere of 5% CO_2 Unless otherwise indicated, HeLa S3 cells were used in most of the cell experiments. HeLa S3 3 × Flag-HA SETD3 knock-in cell line was obtained from previous study (Duan et al., 2024). DNA and siRNAs were transfected using Lipofectamine 2000 (11668–019, Thermo Fisher, USA) and Lipofectamine Hieff Trans (40806ES03, Yeason, Shanghai), respectively, following the manufacturer's protocol. The synthesized siRNA sequences are below: si*hnRNPK*: 5′-UGAAACACUGGCAUUGUAGTT-3’; si*SETD3*: 5′-GGCUUUGGUUUGAGAGCAATT-3’. In response to FCCP (Carbonyl cyanide-4-(trifluoromethoxy) phenylhydrazone)-induced mitochondrial stress, HEK 293T cells were treated with a final concentration of 10 μM for 16 h.

4.2. Plasmids and antibodies

Human *SETD3* was subcloned into a pCS2-3 × Flag vector, and human *hnRNPK* was PCR-amplified and subcloned into the pEGFP or pGEX-4T vector, respectively. The pENTR4-*SETD3* vector was obtained from a cDNA library. Subsequently, an LR recombination reaction (11791020, Invitrogen, USA) was employed to transfer the entry sequence into a destination vector. This destination vector was internally engineered from a pMSCV-puro (PT3303-5, Clontech, USA) plasmid, incorporating an N-terminal Halo tag, followed by 3 × TEV cleavage sites, 2 × StrepII, and a Gateway™ recombination cassette. The sequence of Halo-3 × TEV-2 × StrepII-*SETD3/PTB*-puro was validated through sequencing and then cloned into the pHAGE vector using MultiF Seamless Assembly Mix (RK21020, ABclonal, Wuhan). Antibodies against Flag (20543-1-AP, Proteintech, Wuhan), Flag (F1804, Sigma-Aldrich, USA), GFP (AE012, ABclonal, Wuhan), GAPDH (20943-1-AP, Proteintech, Wuhan), β-Actin (AC026, ABclonal, Wuhan), streptavidin (A0303, Beyotime, Shanghai), TEFB (13372-1-AP, Proteintech, Wuhan), and hnRNPK (11426-1-AP, Proteintech, Wuhan) were purchased. Anti-SETD3 antibody was generated by Du laboratory as described previously (Zhao et al., 2019).

4.3. Co-IP experiments and Western blot

For co-IP experiments, cells were collected and lysed in IP buffer [25 mM Tris-HCl pH 7.4, 150 mM NaCl, 5% glycerol, 1 mM EDTA, and 1% NP-40] containing a protease inhibitor cocktail on ice for 30 min. The Flag resin or GFP resin was added to the lysates and incubated at 4 °C for 4 h or overnight with continuous rotation. After being washed with IP buffer three times, the resins were resuspended in 2 × SDS sample buffer, boiled, and centrifuged at 13,000 rpm for 5 min. Supernatants were subjected to SDS–polyacrylamide gel electrophoresis (SDS-PAGE), transferred to a nitrocellulose membrane, and immunoblotted with the indicated antibodies.

4.4. TurboID assay

HeLa S3 cells expressing Flag-SETD3-TurboID or Flag-TurboID empty vector were incubated with biotin (500 μM) for 2 h, and cell lysates were

subjected to immunoprecipitation in buffer [25 mM Tris-HCl pH 7.4, 150 mM NaCl, 5% glycerol, 1 mM EDTA, and 1% NP-40] containing a protease inhibitor cocktail (B14001, Bimake, Shanghai) using streptavidin resin (35101ES03, Yeason, Shanghai) at 4 °C overnight with rotation. After being washed with 500 mM NaCl IP buffer three times, the resins were resuspended in 2 × SDS sample buffer, boiled, and centrifuged. Samples were separated by SDS-PAGE gel, followed by Coomassie blue staining. The entire gel lane was cut for MS analysis. Samples were analyzed by liquid chromatography–tandem mass spectrometry (LC-MS/MS) on a Q Exactive-HF mass spectrometer (ThermoFisher Scientific). LC-MS/MS data were processed using Proteome Discoverer and searched against the Swiss-Prot *Homo sapiens* protein sequence database. Mass spectrometry data have been deposited to the ProteomeXchange Consortium via the PRIDE Archive with the dataset identifier PXD046472.

4.5. Protein expression and Purification

BL21 (DE3) pTf16–competent cells bearing a plasmid encoding GST-SETD3, His-SETD3, His-SUMO-SETD3, or His-CENP-B were induced by 0.1 mM Isopropyl β-D-Thiogalactoside (IPTG) and L-arabinose (0.5 mg/mL) at 16 °C for 8 h. Cells were lysed in a buffer containing 50 mM Tris-HCl pH 7.5, 150 mM NaCl, and 0.05% NP-40. Proteins were purified using glutathione-sepharose resin (SA008005, Smart Lifesciences, Changzhou) or Ni-magnetic agarose beads (36113, Qiagen, Germany), followed by elution with glutathione [20 mM in 75 mM Tris-HCl pH 8.0] or elution buffer [50 mM NaH_2PO_4, 300 mM NaCl, 250 mM imidazole pH 8.0], respectively. Purified proteins were dialyzed with phosphate buffer saline (PBS) and stored at −80 °C freezer.

4.6. RNA isolation, reverse transcription, and PCR analysis

Total RNAs were extracted with TRIzol (R401-01, Vazyme, Nanjing). cDNAs were synthesized from 1 μg of RNAs using ABScript III RT MasterMix for qPCR with gDNA Remover (RK20429, ABclonal, Wuhan). Taq MasterMix (CW0690M, CWBIO, Jiangsu) was used for exon amplification. qRT-PCR was run using SYBR qPCR master mix (Q331-02, Vazyme, Nanjing). Gene expression levels were normalized to *ACTIN* expression. The primer sequences are listed in Supplemental Table S3.

4.7. RNA-seq, gene expression and alternative splicing analysis

RNA-seq libraries were prepared using 1 μg of total RNA. Polyadenylated RNA isolation, cDNA synthesis, end-repair, ligation of Illumina indexed adapters, and library amplification were completed using the Fast RNA-seq Lib Prep Kit V2 (20306, ABclonal, Wuhan). Libraries were size-selected for 200–300 bp cDNA fragments using VAHTS DNA clean beads (N411-01, Vazyme, Nanjing) and subsequently sequenced on the Illumina NovaSeq 6000 v1.5 reagents (paired-end). Libraries that passed quality control were trimmed using Trim Galore (v0.6.7) and mapped to the human genome GRCh38 using STAR (v2.7.10a). Reads counting was performed using feature counts (v2.0.1). DESeq2 (v1.34.0) was employed to compute differential gene expression using raw read counts as Input. Heatmaps were generated using the pheatmap package (v1.0.12) in R (4.1.2).

Alternative splicing events were analyzed using rMATS software (v4.1.2) with command '-t paired –variable-read-length –tmp tmp –nthread 10 –readLength 150 –od AS'. The significance of change was set using a threshold of $|\Delta\text{IncLevel}| > 0.1$ [$\Delta\text{IncLevel} = \text{IncLevel}_{(siControl)} - \text{IncLevel}_{(siSETD3)}$] and the false discovery rate (FDR) ≤ 0.05 (Shen et al., 2014).

Exon sequence motif analysis requires custom code to extract sequence information corresponding to exon coordinates, followed by the use of MEME (v5.5.6) to calculate and visualize the motifs.

4.8. Quantitative RNA binding assay

The pHAGE-Halo-3 × TEV-2 × StrepII-*SETD3*-puro plasmid, along with pMD2G and pSPAX2, were co-transfected into HEK 293T cells. After 48–72 h post-transfection, media containing viruses were collected. Following infection, puromycin (1 μg/ml) was added to select for stable cell lines. In a typical RNA binding assay, approximately 1×10^7 HEK 293T cells expressing the Halo-PTB or Halo-SETD3 fusion proteins were crosslinked using a UVP crosslinker at UVC (254 nm, 400 mJ/cm^2) (Gu et al., 2018). Crosslinked cells were collected and lysed in 1 mL lysis buffer [50 mM Tris–HCl pH 7.4, 100 mM NaCl, 1 mM DTT, 1% Triton X-100, 10% glycerol] supplemented with 1 × protease inhibitor cocktail on ice for 15 min. Insoluble fractions were removed by centrifugation at maximum speed at 4 °C for 10 min, and the supernatant was incubated with Magne HaloTag Beads (G728A, Promega, USA) at 4 °C for 10–16 h. Beads associated with Halo-*SETD3* complexes were washed with PBST (PBS + 0.1% Triton-X 100), dephosphorylated with calf intestinal phosphatase (M0290S, New England Biolabs, USA) at 37 °C for 30 min. Subsequently, the beads were then washed five times with PNK buffer [50 mM Tris–HCl pH 8.0, 10 mM $MgCl_2$, and 1% Triton X-100]. The beads were treated with buffer containing 8 M guanidine, 8 M urea, and 10% SDS to thoroughly remove non-covalent contaminants. The *SETD3*-RNA complexes were then cleaved off from the beads using TEV protease and digested with proteinase K (RO02503LQ, ABclonal, Wuhan) at 37 °C for 30 min. Bound RNA was quantified by reading OD_{260} using a spectrometer.

4.9. ChIP-seq assay

ChIP assay was performed as previously described (Geng et al., 2023). Briefly, Cells were cross-linked in 1% formaldehyde for 10 min and subsequently quenched with 0.125 M glycine for 5 min. After being washed with cold PBS twice, cells were lysed in cell lysis buffer [50 mM PIPES pH 8.0, 85 mM KCl, 0.5% NP-40] on ice for 20 min, followed by incubation of nuclei lysis buffer [50 mM Tris-HCl pH 8.0, 10 mM EDTA, 1% Triton X-100] at 4 °C for 20 min. Cells were sonicated using a bioruptor (Minichiller 300, Diagenode) with 30 cycles (30 s-on, 30 s-off). The supernatant was then incubated with 2 μg of HA (66006-2-Ig, Proteintech, Wuhan) antibody at 4 °C overnight. Subsequently, 15 μl of ChIP-grade protein A/G magnetic beads (26162, Thermo Scientific, USA) were added to the solution and incubated at 4 °C for 1.5 h. Beads were washed with washing buffer [250 mM LiCl, 10 mM Tris-HCl, 1 mM EDTA, 1% NP-40, 1% sodium deoxycholate] four times and eluted with elution buffer [10 mM NaHCO3, 1% SDS] twice before de-crosslinked with proteinase K (1.5 mg/mL) at 65 °C overnight. DNA was extracted using Universal DNA Purification Kit (DP214-03, Tiange, Beijing). ChIP-seq libraries were generated using the VAHTS™ Universal DNA Library Prep Kit for Illumina® V3 and sequenced according to the NovaSeq 6000 protocol.

Sequencing adapters were trimmed using Trim Galore (v0.6.7). The clean reads were mapped to the human genome GRCh38 using STAR (v2.7.11b) with the parameters –runThreadN 16 –runMode alignReads –readFilesCommand zcat –quantMode TranscriptomeSAM GeneCounts –twopassMode Basic –outSAMtype BAM SortedByCoordinate –outSAMunmapped None. Duplicate reads were removed using Sambamba (v1.0.0). Deeptools (v3.5.5) was employed to visualize the SETD3 and CENP-B signals after normalization. Peaks were called using Macs2 (v2.1.1). Circos (v0.69–8) was used to plot the circular peak plot.

4.10. EMSA

The following 20 μL reaction system was prepared on ice: 10 × binding buffer [100 mM Tris-HCl pH 7.5, 10 mM EDTA, 1 M KCl, 1 mM DTT, 50% Glycerol], 100 ng DNA, 1 μg protein and sterile H_2O. Different recombinant proteins were incubated with synthetic double strand DNA (dsDNA) at 25 °C for 60 min. The mixtures were individually

added with 5 × native sample buffer and subjected to PAGE. The separated components were then transferred to a nylon membrane and immunoblotted with the indicated antibodies. The synthetic DNA sequences are the sequences of α-satellite monomers H, shown as previously (Logsdon et al., 2021).

4.11. In vitro methyltransferase assay

In vitro methyltransferase reactions were performed with 5 μg methyltransferase, 1 μg substrate, and 2 μCi ^{3}H-S-adenosyl-L-methionine in reaction buffer [50 mM Tris-HCl pH 8.0, 20 mM KCl, 5 mM $MgCl_2$] at 30 °C overnight. Reactions were spotted onto Whatman P81 filters and washed four times with 50 mM $NaHCO_3$, pH 9.0 before scintillation counting.

4.12. PLA

Unless statement, all procedures were conducted at room temperature. HeLa S3 cells were cultured on glass coverslips at 37 °C, then washed twice with PBS, fixed with 3.7% paraformaldehyde for 10 min. After permeabilization with 0.3% Triton X-100 for 10 min, cells were blocked with 5% BSA in PBST buffer and incubated for 30 min. Cells were subsequently incubated with the indicated primary antibody either at room temperature for 2 h or at 4 °C overnight. PLA experiments were performed using the Duolink PLA kits (DUO92101, Sigma-Aldrich, USA) following the manufacturer's protocol. The coverslips were stained with 4′,6′-diamidino-2-phenylindole (DAPI) and mounted. Immunofluorescence images were captured using a confocal laser scanning microscope (Leica SP8).

4.13. Protein molecular docking

ZDOCK (v3.0.2) software was used to predict the interactions between SETD3 and hnRNPK. The structures of SETD3 and hnRNPK were download from AlphaFold Protein Structure Database. The highest-scoring model was shown, and its Gibbs free energy (ΔG) was calculated using PDBePISA, with any possible formation of hydrogen bonds. The dissociation constant (K_d) was calculated by the following thermodynamic equation: $\Delta G = RT\ ln(Kd)$. The representative image generated by Pymol (v2.1.0) displays the local structure of the SETD3-hnRNPK interaction.

4.14. Statistical analysis

Unless otherwise indicated, data are presented as the mean ± SD from three biological replicates, and the differences between any two groups were compared by unpaired Student's *t*-test. Data were plotted using Prism 9 software. $^{*}P < 0.05$, $^{**}P < 0.01$, $^{***}P < 0.001$, $^{****}P < 0.0001$, and ns indicates “not significant”.

Supporting information

The raw RNA-Seq and ChIP-seq data have been deposited in the Genome Sequence Archive in National Genomics Data Center (Members and Partners, 2022), China National Center for Bioinformation / Beijing Institute of Genomics, Chinese Academy of Sciences (GSA-Human: HRA007736 and HRA008305) that are publicly accessible at https://ngdc.cncb.ac.cn/gsa-human.

CRediT authorship contribution statement

Yue-Yu Kong: Writing – review & editing, Writing – original draft, Visualization, Validation, Resources, Methodology, Formal analysis, Data curation, Conceptualization. **Wen-Jie Shu:** Writing – review & editing, Resources, Methodology, Formal analysis, Data curation, Conceptualization. **Shuang Wang:** Writing – review & editing, Validation, Resources, Methodology, Formal analysis, Data curation. **Zhao-Hong Yin:** Writing – review & editing, Validation, Methodology, Data curation. **Hongguo Duan:** Writing – review & editing, Resources, Formal analysis. **Ke Li:** Data curation. **Hai-Ning Du:** Writing – review & editing, Writing – original draft, Visualization, Validation, Supervision, Resources, Project administration, Methodology, Investigation, Funding acquisition, Formal analysis, Data curation, Conceptualization.

Declaration of competing interest

The authors declare that they have no known competing financial interests or personal relationships that could have appeared to influence the work reported in this paper.

Acknowledgements

The authors are grateful to Dr. Ming Ding (China Pharmaceutical University) for the assistance of mass spectrometry, Dr. Yang Yu (Institute of Biophysics, Chinese Academy of Sciences) and Dr. Rui Xiao (Wuhan University) for plasmids, Dr. Zhiyin Song (Wuhan University) for reagents, Dr. Yongzhen Xu (Wuhan University) for helpful discussion, and Ms. Yuan-Xin Ye (Hubei University of Technology) for drawing of graphical abstract. This work was supported by the grants from the National Natural Science Foundation of China (31971231 and 32270617), the National Key R&D program of China (2023YF0913403), and the Fundamental Research Funds for the Central Universities (2042022dx0003).

Appendix A. Supplementary data

Supplementary data to this article can be found online at https://doi.org/10.1016/j.cellin.2024.100198.

References

Abaev-Schneiderman, E., Admoni-Elisha, L., & Levy, D. (2019). SETD3 is a positive regulator of DNA-damage-induced apoptosis. *Cell Death & Disease, 10*(2), 74.
Admoni-Elisha, L., et al. (2022). Structure-function conservation between the methyltransferases SETD3 and SETD6. *Biochimie, 200*, 27–35.
Alganatay, C., et al. (2024). SETD3 regulates endoderm differentiation of mouse embryonic stem cells through canonical Wnt signaling pathway. *The FASEB Journal, 38*(4), Article e23463.
Bhattacharya, S., et al. (2021). The methyltransferase SETD2 couples transcription and splicing by engaging mRNA processing factors through its SHI domain. *Nature Communications, 12*(1), 1443.
Black, J. C., Van Rechem, C., & Whetstine, J. R. (2012). Histone lysine methylation dynamics: Establishment, regulation, and biological impact. *Molecular Cell, 48*(4), 491–507.
Busch, A., & Hertel, K. J. (2012). Evolution of SR protein and hnRNP splicing regulatory factors. *Wiley Interdiscip Rev RNA, 3*(1), 1–12.
Cai, Z., et al. (2020). RIC-seq for global in situ profiling of RNA-RNA spatial interactions. *Nature, 582*(7812), 432–437.
Cao, R., et al. (2018). Molecular basis for histidine N1 position-specific methylation by CARNMT1. *Cell Research, 28*(4), 494–496.
Cheng, X., et al. (2017). Cell cycle-dependent degradation of the methyltransferase SETD3 attenuates cell proliferation and liver tumorigenesis. *Journal of Biological Chemistry, 292*(22), 9022–9033.
Cornett, E. M., et al. (2019). Lysine methylation regulators moonlighting outside the epigenome. *Molecular Cell, 75*(6), 1092–1101.
Davydova, E., et al. (2021). The methyltransferase METTL9 mediates pervasive 1-methylhistidine modification in mammalian proteomes. *Nature Communications, 12*(1), 891.
Diep, J., et al. (2019). Enterovirus pathogenesis requires the host methyltransferase SETD3. *Nat Microbiol, 4*(12), 2523–2537.
Duan, H., et al. (2024). SETD3-mediated histidine methylation of MCM7 regulates DNA replication by facilitating chromatin loading of MCM. *Science China Life Sciences*. http://engine.scichina.com/doi/10.1007/s11427-023-2600-0.
Earnshaw, W. C., & Rothfield, N. (1985). Identification of a family of human centromere proteins using autoimmune sera from patients with scleroderma. *Chromosoma, 91*(3–4), 313–321.
Escobar-Hoyos, L. F., et al. (2020). Altered RNA splicing by mutant p53 activates oncogenic RAS signaling in pancreatic cancer. *Cancer Cell, 38*(2), 198–211 e198.
Escobar-Hoyos, L., Knorr, K., & Abdel-Wahab, O. (2019). Aberrant RNA splicing in cancer. *Annual Review of Cell Biology, 3*(1), 167–185.

Feng, Y., et al. (2022). Up-regulation of SETD3 may contribute to post-stroke depression in rat through negatively regulating VEGF expression. *Behavioural Brain Research, 416*, Article 113564.
Geng, Q., et al. (2023). Dynamic phosphorylation of G9a regulates its repressive activity on chromatin accessibility and mitotic progression. *Advanced Science, 10*(30), Article e2303224.
Geuens, T., Bouhy, D., & Timmerman, V. (2016). The hnRNP family: Insights into their role in health and disease. *Human Genetics, 135*(8), 851–867.
Gu, J., et al. (2018). GoldCLIP: Gel-omitted ligation-dependent CLIP. *Genomics, Proteomics & Bioinformatics, 16*(2), 136–143.
Guo, Q., et al. (2019). Structural insights into SETD3-mediated histidine methylation on beta-actin. *Elife, 8*.
Han, N., Li, W., & Zhang, M. (2013). The function of the RNA-binding protein hnRNP in cancer metastasis. *Journal of Cancer Research and Therapeutics, 9*(Suppl), S129–S134.
Hassan, N., et al. (2020). SETD3 acts as a prognostic marker in breast cancer patients and modulates the viability and invasion of breast cancer cells. *Scientific Reports, 10*(1), 2262.
Herz, H. M., Garruss, A., & Shilatifard, A. (2013). SET for life: Biochemical activities and biological functions of SET domain-containing proteins. *Trends in Biochemical Sciences, 38*(12), 621–639.
Husmann, D., & Gozani, O. (2019). Histone lysine methyltransferases in biology and disease. *Nature Structural & Molecular Biology, 26*(10), 880–889.
Jakobsson, M. E. (2021). Enzymology and significance of protein histidine methylation. *Journal of Biological Chemistry, 297*(4), Article 101130.
Kwiatkowski, S., et al. (2018). SETD3 protein is the actin-specific histidine N-methyltransferase. *eLife, 7*.
Li, W. J., et al. (2021). Profiling PRMT methylome reveals roles of hnRNPA1 arginine methylation in RNA splicing and cell growth. *Nature Communications, 12*(1), 1946.
Logsdon, G. A., et al. (2021). The structure, function and evolution of a complete human chromosome 8. *Nature, 593*(7857), 101–107.
Malik, N., et al. (2023). Induction of lysosomal and mitochondrial biogenesis by AMPK phosphorylation of FNIP1. *Science, 380*(6642), Article eabj5559.
Members, C.-N., & Partners. (2022). Database Resources of the national genomics data center, China national center for bioinformation in 2022. *Nucleic Acids Research, 50*(D1), D27–D38.
Mendel, M., et al. (2021). Splice site m(6)A methylation prevents binding of U2AF35 to inhibit RNA splicing. *Cell, 184*(12), 3125–3142 e3125.
Muro, Y., et al. (1992). Centromere protein B assembles human centromeric alpha-satellite DNA at the 17-bp sequence, CENP-B box. *The Journal of Cell Biology, 116*(3), 585–596.
Ostrowski, J., et al. (2004). Heterogeneous nuclear ribonucleoprotein K enhances insulin-induced expression of mitochondrial UCP2 protein. *Journal of Biological Chemistry, 279*(52), 54599–54609.
Paziewska, A., et al. (2004). Cooperative binding of the hnRNP K three KH domains to mRNA targets. *FEBS Letters, 577*(1–2), 134–140.
Pires-Luis, A. S., et al. (2015). Expression of histone methyltransferases as novel biomarkers for renal cell tumor diagnosis and prognostication. *Epigenetics, 10*(11), 1033–1043.
Rogalska, M. E., Vivori, C., & Valcarcel, J. (2023). Regulation of pre-mRNA splicing: Roles in physiology and disease, and therapeutic prospects. *Nature Reviews Genetics, 24*(4), 251–269.
Sachamitr, P., et al. (2021). PRMT5 inhibition disrupts splicing and stemness in glioblastoma. *Nature Communications, 12*(1), 979.
Sessa, A., et al. (2019). SETD5 regulates chromatin methylation state and preserves global transcriptional fidelity during brain development and neuronal wiring. *Neuron, 104*(2), 271–289 e213.
Shen, S., et al. (2014). rMATS: robust and flexible detection of differential alternative splicing from replicate RNA-Seq data. *Proceedings of the National Academy of Sciences of the U S A, 111*(51), E5593–E5601.
Shimazu, T., et al. (2023). Histidine N1-position-specific methyltransferase CARNMT1 targets C3H zinc finger proteins and modulates RNA metabolism. *Genes & Development, 37*(15–16), 724–742.
Shnyreva, M., et al. (2000). Interaction of two multifunctional proteins. Heterogeneous nuclear ribonucleoprotein K and Y-box-binding protein. *Journal of Biological Chemistry, 275*(20), 15498–15503.
Shu, W. J., & Du, H. N. (2021). The methyltransferase SETD3-mediated histidine methylation: Biological functions and potential implications in cancers. *Biochimica et Biophysica Acta (BBA) - Reviews on Cancer, 1875*(1), Article 188465.
Wilkinson, A. W., et al. (2019). SETD3 is an actin histidine methyltransferase that prevents primary dystocia. *Nature, 565*(7739), 372–376.
Wright, C. J., Smith, C. W. J., & Jiggins, C. D. (2022). Alternative splicing as a source of phenotypic diversity. *Nature Reviews Genetics, 23*(11), 697–710.
Xu, L., et al. (2019). SETD3 is regulated by a couple of microRNAs and plays opposing roles in proliferation and metastasis of hepatocellular carcinoma. *Clinical Science, 133*(20), 2085–2105.
Yoo, Y., et al. (2006). Interaction of N-WASP with hnRNPK and its role in filopodia formation and cell spreading. *Journal of Biological Chemistry, 281*(22), 15352–15360.
Zhang, X., Huang, Y., & Shi, X. (2015). Emerging roles of lysine methylation on non-histone proteins. *Cellular and Molecular Life Sciences, 72*(22), 4257–4272.
Zhao, M. J., et al. (2019). MiR-15b and miR-322 inhibit SETD3 expression to repress muscle cell differentiation. *Cell Death & Disease, 10*(3), 183.
Zhao, W., et al. (2023). Molecular basis for protein histidine N1-specific methylation of the "His-x-His" motifs by METTL9. *Cell Insight, 2*(3), Article 100090.
Zheng, Y., Zhang, X., & Li, H. (2020). Molecular basis for histidine N3-specific methylation of actin H73 by SETD3. *Cell Discov, 6*, 3.
Zou, T., et al. (2022). Stabilization of SETD3 by deubiquitinase USP27 enhances cell proliferation and hepatocellular carcinoma progression. *Cellular and Molecular Life Sciences, 79*(1), 70.